Vibronic coupling and double excitations in linear response time-dependent density functional calculations: dipole-allowed states of N2

Neugebauer, J.; Baerends, E.J.; Nooijen, M.A.Th.F.

published in
Journal of Chemical Physics
2004

DOI (link to publisher)
10.1063/1.1785775

document version
Publisher's PDF, also known as Version of record

citation for published version (APA)
Neugebauer, J., Baerends, E. J., & Nooijen, M. A. T. F. (2004). Vibronic coupling and double excitations in linear response time-dependent density functional calculations: dipole-allowed states of N2. *Journal of Chemical Physics*, *121*(13), 6155-66. https://doi.org/10.1063/1.1785775

Vibronic coupling and double excitations in linear response time-dependent density functional calculations: Dipole-allowed states of N_2

Johannes Neugebauer[a] and Evert Jan Baerends[b]
Theoretical Chemistry, Vrije Universiteit Amsterdam, De Boelelaan 1083, 1081 HV Amsterdam, The Netherlands

Marcel Nooijen[c]
Department of Chemistry, University of Waterloo, 200 University Avenue West, Waterloo, Ontario N2L 3G1, Canada

(Received 24 May 2004; accepted 1 July 2004)

The present study serves two purposes. First, we evaluate the ability of present time-dependent density functional response theory (TDDFRT) methods to deal with avoided crossings, i.e., vibronic coupling effects. In the second place, taking the vibronic coupling effects into account enables us, by comparison to the configuration analysis in a recent *ab initio* study [J. Chem. Phys. **115**, 6438 (2001)], to identify the neglect of double excitations as the prime cause of limited accuracy of these linear response based TDDFRT calculations for specific states. The ''statistical averaging of (model) orbital potentials (SAOP)'' Kohn–Sham potential is used together with the standard adiabatic local-density approximation (ALDA) for the exchange-correlation kernel. We use the N_2 molecule as prototype, since the TDDFRT/SAOP calculations have already been shown to be accurate for the vertical excitations, while this molecule has a well-studied, intricate vibronic structure as well as significant double excitation nature in the lowest $^1\Pi_u$ state at elongated bond lengths. A simple diabatizing scheme is employed to obtain a diabatic potential energy matrix, from which we obtain the absorption spectrum of N_2 including vibronic coupling effects. Considering the six lowest dipole allowed transitions of $^1\Sigma_u^+$ and $^1\Pi_u$ symmetry, we observe a good general agreement and conclude that avoided crossings and vibronic coupling can indeed be treated satisfactorily on the basis of TDDFRT excitation energies. However, there is one state for which the accuracy of TDDFRT/ALDA clearly breaks down. This is the state for which the *ab initio* calculations find significant double excitation character. To deal with double excitation character is an important challenge for time-dependent density functional theory. © *2004 American Institute of Physics.*
[DOI: 10.1063/1.1785775]

I. INTRODUCTION

The absorption spectrum of N_2 is a difficult test case for current quantum-chemical methods because of the irregular vibronic structure.[1,2] Several interacting electronic states play a role, so that even the description of vertical excitation energies is a problematic task. The difficult fine structure of the electronic spectrum has been explained in terms of three interacting diabatic states of $^1\Sigma_u^+$ symmetry and again three of $^1\Pi_u$ symmetry,[3,4] and many experimental studies have been performed in order to determine the complicated intensity distribution over the vibronic levels (see, e.g., Refs. 1, 2 and 5 and references therein). In particular Chan *et al.*[1] describe the difficulties in the measurements of not only absolute, but also *relative* oscillator strengths for this system, which serve as a basis for all empirical deductions of parameters to simulate the absorption spectra. In 1983, Stahel, Leoni, and Dressler[6] presented a quantitative model for the couplings between the diabatic states, where the parameters for their model were fitted to experimental spectroscopic constants. In 2001, Spelsberg and Meyer[7] performed a detailed study, using multireference configuration-interaction (MR-CI) calculations to obtain adiabatic and diabatic potential energy curves for the lowest $^1\Sigma_u^+$ and $^1\Pi_u$ states. Because of the high sensitivity of the resulting spectra to the calculated potential energy curves, an empirical fitting procedure is employed in their study to reproduce the experimental details of the absorption spectrum. It turned out that mainly vertical shifts in the potential energy curves are necessary to achieve agreement between the calculated and experimental spectra. This definitive study is used as a benchmark in the present work.

Besides these attempts to model the fine structure of the absorption spectrum, several *first-principles* calculations of vertical excitation energies for N_2 have been performed, including polarization-propagator and equation-of-motion techniques,[8] multireference coupled-cluster (MR-CC),[9] equation-of-motion coupled-cluster (EOM-CC),[10] and density functional theory (DFT) calculations employing asymptotically corrected potentials,[11–13] as well as calculations using the size-consistent self-consistent $(SC)^2$ intermediate Hamiltonian approach to CI calculations, $(SC)^2CI$.[14]

A picture of the diabatic potential energy curves that

[a]Electronic mail: jneugeb@chem.vu.nl
[b]Electronic mail: baerends@chem.vu.nl
[c]Electronic mail: nooijen@uwaterloo.ca

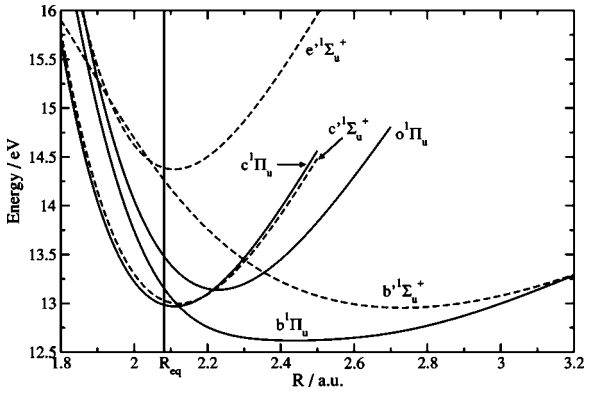

FIG. 1. Sketch of the diabatic potential energy curves for the three lowest states of $^1\Pi_u$ (solid lines) and $^1\Sigma_u^+$ symmetry (dashed lines). These curves have been obtained from the set of recommended parameters in Ref. 7 and are in agreement with experimental observations. For better comparison with our data, the curves are shifted by our ground-state zero-point kinetic energy (0.146 eV), while the original curves are given relative to the $v=0$ level of the ground state.

have been obtained from the set of recommended parameters given in Ref. 7 is shown in Fig. 1. The state with the lowest minimum, which is rather shallow, is denoted $b\,^1\Pi_u$. Its low frequency has been considered indicative of a valence excited character: $2\sigma_u \rightarrow 1\pi_g$. From Fig. 1 it can be seen that the diabatic $b\,^1\Pi_u$ with this valence character should be the second lowest $^1\Pi_u$ state at the ground state equilibrium distance R_{eq}. However, in many of the calculations in the literature, the $2\sigma_u \rightarrow 1\pi_g$ valence excitation is predicted to be, at R_{eq}, at higher energies than both other $^1\Pi_u$ states. In particular the results from calculations using the statistical averaging of (model) orbital potentials[15–17] (SAOP) in Ref. 13 raised the question whether a different assignment should be made, the calculated vertical excitations being in very good agreement (errors $\leqslant$0.16 eV for all three investigated $^1\Pi_u$ states and all but one of the three $^1\Sigma_u^+$ states in comparison to the experimental values from Ref. 1) when it is assumed that the $2\sigma_u \rightarrow 1\pi_g$ valence excitation corresponds, at R_{eq}, to the highest of the three states of $^1\Pi_u$ symmetry, $o\,^1\Pi_u$. The implication would be that according to the calculations the two lowest states of $^1\Pi_u$ symmetry have Rydberg character. The question acquires special significance since Spelsberg and Meyer[7] have found that the $b\,^1\Pi_u$ has significant double excitation character, which even predominates at longer bond distances. Their results support the original assignment, and suggest that the time-dependent density functional response theory (TDDFRT) calculations are indeed significantly in error for the $2\sigma_u \rightarrow 1\pi_g$ valence excited state, putting it at too high energy because they are unable to incorporate this double excitation character.

In the present study the adiabatic potential energy curves of N_2 are generated with TDDFRT/SAOP calculations. A diabatizing scheme following Ref. 18 is applied to obtain a Taylor-series expansion of an effective Hamiltonian in a diabatic basis, from which diabatic potential energy curves can be obtained. This effective Hamiltonian is also used to calculate the fine structure of the electronic absorption spectrum of N_2, including the vibronic couplings between the diabatic model potential energy curves for the $^1\Sigma_u^+$ states, and separately for the $^1\Pi_u$ states. By comparison of these results with experiment and with the high-level MR-CI calculations from Ref. 7 we demonstrate with the $^1\Sigma_u^+$ results the feasibility of vibronic coupling calculations on the basis of adiabatic TDDFRT energy curves exhibiting avoided crossings. In the $^1\Pi_u$ case we will show that the vibronic coupling calculations vindicate the original assignment of the lowest vibronic levels to the valence excited state. The suggested alternative assignment, that they might be due to vibronically coupled Rydberg states, is not tenable. This implies that there is, in this case, a deviation of the TDDFRT/SAOP vertical excitation energy from experiment by much more than 0.1 eV already at R_{eq}, which becomes even worse at longer bond distances. We trace this ''failure'' of TDDFRT/SAOP calculations in this case to the significant double excitation character of the valence excited $b\,^1\Pi_u$ state, which is not properly represented within linear response theory. Additional calculations using the similarity-transformed (ST) EOM-CC (Refs. 19–25) and the extended-STEOM-CC (Ref. 26) methods support the importance of doubly excited configurations for this state. The possibility that insufficiencies in the SAOP functional for the Kohn–Sham potential could be held responsible, is ruled out by calculations using highly accurate Kohn–Sham potentials based on correlated *ab initio* densities, which lead to similar discrepancies.

II. METHODOLOGY

Density functional calculations have been performed using a modified version of the Amsterdam density functional (ADF) package.[27,28] We used the SAOP potential[15–17] in combination with the even-tempered ET-QZ3P-3DIFFUSE basis set from the ADF basis set library[27] including three sets of diffuse functions to calculate TDDFRT solution vectors and vertical excitation energies for structures displaced along the normal coordinates. Details of the basis can be found in Ref. 13. For ground-state structure optimization, frequency analysis, and reference energy calculations, we employed the Becke–Perdew–Wang exchange-correlation functional, dubbed BPW91;[29,30] test calculations showed that other generalized-gradient approximations to the exact exchange-correlation functional yield very similar results.

The construction of diabatic states and effective Hamiltonians follows the approach in Ref. 18 (for introductions to vibronic coupling calculations see also Refs. 31–33). According to the short-time approximation for absorption and resonance Raman scattering (see, e.g., Refs. 31, 34–37), one needs to accurately model the potential energy curves correctly near the ground-state equilibrium structure in order to obtain a good description of spectroscopic properties. Therefore, we identify adiabatic and diabatic states at a reference geometry, usually the ground-state equilibrium geometry, and determine the diabatic states for geometries displaced along the normal coordinate in such a way that they resemble the electronic states at the reference geometry. This scheme is related to the determination of matrix elements between diabatic states by wave function coefficients[38,39] instead of using molecular properties to define the adiabatic↔diabatic transformation.[7,40]

The effective Hamiltonian consists of the kinetic energy operator for the nuclei and a potential energy matrix in the diabatic basis. For the latter, we use a second-order Taylor series expansion around the equilibrium structure,

$$\mathbf{V}(\mathbf{q})=\mathbf{V}(0)+\sum_{i=1}^{N_q}\left(\frac{\partial \mathbf{V}}{\partial q_i}\right)_0 q_i+\frac{1}{2}\sum_{i,j=1}^{N_q}\left(\frac{\partial^2 \mathbf{V}}{\partial q_i\,\partial q_j}\right)_0 q_i\,q_j, \quad (1)$$

where q_i are the normal coordinates of the system. Of course, this general expression for a multimode system reduces to a much simpler form for N_2, since only one normal coordinate has to be considered. The derivatives of the potential energy matrix with respect to (w.r.t.) the normal coordinates are calculated in ADF by numerical differentiation of diabatic potential energy matrices for displaced structures, $\mathbf{V}(\pm\Delta q)$. Each of those diabatic matrices is constructed by a unitary transformation of the diagonal adiabatic potential energy matrix containing the vertical excitation energies for that particular structure,

$$\mathbf{V}(q)=\mathbf{U}^{\dagger}(q)\mathbf{E}^{\mathrm{elec}}(q)\mathbf{U}(q). \quad (2)$$

The vertical excitation energies and, therefore, also the diagonal matrix $\mathbf{E}^{\mathrm{elec}}(q)$ are known from the TDDFT calculation. The transformation matrices $\mathbf{U}(q)$ are calculated in such a way that the overlap matrix of the adiabatic excited state wave functions is almost diagonal, which ensures that the diabatic wave functions at the displaced structures are similar in character to the wave functions at the reference structure.

In the framework of TDDFRT, a related quantity is the overlap between (modified) adiabatic transition densities,

$$S_{AB}^{\mathrm{adiab}}(\Delta q)=\langle\overline{\rho}^{A}(0)|\overline{\rho}^{B}(\Delta q)\rangle \quad (3)$$

$$=\sum_{i,r}\sum_{j,s}X_{ir}^{\mathrm{MO},A}(0)X_{js}^{\mathrm{MO},B}(\Delta q)\times\langle\phi_i(0)|\phi_j(\Delta q)\rangle\langle\phi_r(0)|\phi_s(\Delta q)\rangle, \quad (4)$$

where the modified transition densities $\overline{\rho}^{A}$ are defined in terms of the elements $X_{ir}^{\mathrm{MO},A}$ of the TDDFRT solution vectors ($\vec{F}$ in Refs. 41 and 42) and the molecular orbitals,

$$\overline{\rho}^{A}=\sum_{ir}X_{ir}^{\mathrm{MO},A}\phi_r\phi_i^{*}. \quad (5)$$

In these equations *A*, *B* label excited electronic states, *i*, *j* label occupied, and *r*, *s* unoccupied molecular orbitals.

Since the molecular orbitals (MO) themselves might undergo changes w.r.t. the reference structure, the calculation of $\mathbf{S}^{\mathrm{adiab}}$ is carried out in terms of the atomic orbital (AO) basis,

$$S_{AB}^{\mathrm{adiab}}(\Delta q)=\sum_{\mu\nu\lambda\rho}X_{\mu\nu}^{\mathrm{AO},A}(0)X_{\lambda\rho}^{\mathrm{AO},B}(\Delta q)S_{\mu(0)\lambda(\Delta q)}^{\mathrm{AO}}S_{\nu(0)\rho(\Delta q)}^{\mathrm{AO}}, \quad (6)$$

where $S_{\mu(0)\lambda(\Delta q)}^{\mathrm{AO}}$ are overlap integrals over AO basis functions,

$$X_{\mu\nu}^{\mathrm{AO},A}(0)=\sum_{i,r}X_{ir}^{\mathrm{MO},A}(0)c_{\mu i}(0)c_{\nu r}(0) \quad (7)$$

are the TDDFRT solution vectors transformed to the AO basis, $c_{\mu i}$ are the MO coefficients, and μ, ν, λ, ρ label atomic basis functions at the reference (0) or displaced (Δq) structures. As is done in Ref. 18 the overlap matrix $\mathbf{S}^{\mathrm{AO}}$ is approximated by the corresponding overlap matrix for the equilibrium structure, since the displacements from the equilibrium structure are very small.

The transformation matrix is then determined in such a way that the corresponding *diabatic* overlap matrix is almost diagonal,

$$S_{AB}^{\mathrm{diab}}(\Delta q)=\sum_{C}U_{BC}(\Delta q)S_{AC}^{\mathrm{adiab}}(\Delta q)\approx\delta_{AB}. \quad (8)$$

This equation defines the matrix $\mathbf{U}(\Delta q)$ and, thus, the diabatic potential energy matrix.

The vibronic coupling simulations based on the diabatic potential energy matrix are carried out using the program package VIBRON.[43]

III. VERTICAL EXCITATIONS

Vertical excitation energies have been calculated for the BPW91/ET-QZ3P-3DIFFUSE optimized structure (bond distance 2.0814 bohr, 110.14 pm) using SAOP/ET-QZ3P-

TABLE I. Vertical excitation energies $E_{\mathrm{excit.}}$ (in eV) and oscillator strengths *f* (in a.u.) from SAOP for dipole-allowed transitions of N_2 using the ET-QZ3P-3DIFFUSE basis set. Experimental values (Refs. 1 and 6) are given for comparison (see text for further explanations). The assignment of orbital transitions is according to inferences from experiment and from MRCI in Ref. 7. Note that the experimental values from Ref. 1 served as a reference for the proposal of the alternative assignment in Ref. 13.

	Experiment			SAOP calculations		
	$E_{\mathrm{excit.}}$		Assigned orbital		Oscillator strengths	Alternative
Label	Fit[a]	Ref. 1	character	E_{excit}	*f*	assignment[b]
$c\,^1\Pi_u$	12.90	13.2	$3\sigma_g\rightarrow 2\pi_u$(Ry)	12.96	0.062 87	13.16 ($1\pi_u\rightarrow 4\sigma_g$,Ry)
$b\,^1\Pi_u$	13.24	12.8	$2\sigma_u\rightarrow 1\pi_g$(val)	13.56	0.083 93	12.96 ($3\sigma_g\rightarrow 2\pi_u$,Ry)
$o\,^1\Pi_u$	13.63	13.6	$1\pi_u\rightarrow 4\sigma_g$(Ry)	13.16	0.091 84	13.56 ($2\sigma_u\rightarrow 1\pi_g$,val)
$c'\,^1\Sigma_u^+$	12.98	12.9	$3\sigma_g\rightarrow 3\sigma_u$(Ry)	12.92	0.221 34	
$b'\,^1\Sigma_u^+$	14.25	14.2	$1\pi_u\rightarrow 1\pi_g$(val)	14.04	0.436 61	
$e'\,^1\Sigma_u^+$	14.48	14.4	$3\sigma_g\rightarrow 4\sigma_u$(Ry)	15.27	0.004 46	

[a]Reference 6.
[b]Reference 13.

TABLE II. Vertical excitation energies (in eV) from SAOP for dipole-allowed transitions of N_2 in comparison to results from *ab initio* calculations and to experimental values (Refs. 6) (see text for further explanations). Note that the assignment in case of MR-CCSD is not unambiguous and has been interpreted in different ways (Refs. 12 and 14).

Label	Expt. fit[a]	SAOP	HCTH(AC) Ref. 12	$(SC)^2$ CAS Ref. 14	MR-CCSD Ref. 9	EOM-CC Ref. 10
$c\ ^1\Pi_u$	12.90	12.96	12.45	12.86	12.842	13.228
$b\ ^1\Pi_u$	13.24	13.56	13.50	13.52	13.714	13.622
$o\ ^1\Pi_u$	13.63	13.16	12.90	13.45	13.608	13.673
$c'\ ^1\Sigma_u^+$	12.98	12.92	12.47	12.83	12.819	12.842
$b'\ ^1\Sigma_u^+$	14.25	14.04	13.93	14.33	14.308	14.573
$e'\ ^1\Sigma_u^+$	14.48	15.27	14.14	14.61	14.653	···

[a]Reference 6.

3DIFFUSE. They are presented in Table I in comparison to experimental values. For the optimization as well as for the calculation of excitation energies, linear dependencies have been removed from the basis set. As expected, the SAOP excitation energies obtained here agree well with those presented in Ref. 13. Differences are due to the slightly different structures employed in the calculations.

Experimental data for vertical excitation energies are not unambiguous, since there is a pronounced vibronic structure in the experimental spectrum, including many overlapping vibrational progressions and couplings between different electronic states. There are two sets of experimental values given in Table I; the first is based on the analysis by Stahel, Leoni, and Dressler,[6] who obtained the diabatic states from a fitting procedure to experimental data. These data are in good agreement with diabatic state energies at R_{eq} which can be extracted from the MR-CI data in Fig. 1. The second set of experimental values is taken from the experimental study in Ref. 1, where the most intense peaks were taken as approximate vertical excitation energies. The uncertainties in the latter values are at least as large as the vibrational spacings in the spectra, i.e., between 0.075 eV for the $b\ ^1\Pi_u$ state and 0.300 eV for the $c\ ^1\Pi_u$ state. The orbital assignment of the experimental data, which we adopt in this work, is based on the work by Dressler[3] and Carroll and Collins.[4] The SAOP excitation energies are generally in good agreement with the experimental values from Ref. 6; considerable deviations of 0.5–0.8 eV are observed only for the $1\pi_u \rightarrow 4\sigma_g$ and the $3\sigma_g \rightarrow 4\sigma_u$ transitions. The experimental determination of the latter value seems to be quite difficult in view of the complicated structure of the N_2 absorption spectrum in this energy range and the low oscillator strength of this transition, making a deconvolution into contributions of at least three different electronic states necessary. We also quote in the table the alternative assignment of the orbital transitions to the experimentally observed states, which as noted by Grüning *et al.*[13] and mentioned in the Introduction, would considerably improve the agreement of the calculations with the experimental vertical excitation energies from the more recent Ref. 1.

In Table II we compare our results to those of several other first-principles studies,[9,10,12,14] sticking to the standard orbital assignments for the experimental states. Not only SAOP, but all high-quality *ab initio* calculations and the TD-DFRT calculation of Ref. 12 yield about the same energy (between 13.50 and 13.71) for the $2\sigma_u \rightarrow 1\pi_g$ valence transition, much higher than the experimental $b\ ^1\Pi_u$ state. As pointed out in Ref. 13 this would mean that SAOP and other asymptotically correct potentials like BP-GRAC and HCTH(AC) as well as many *ab initio* methods all overestimate the vertical excitation energy for this transition by 0.3–0.5 eV if the experimental assignment is correct.

It has been well established (cf. references in Ref. 26) that the *ab initio* MR-CCSD and the EOM-CCSD methods are not well suited to describe states with substantial double excitation character. To investigate the possible effect of double excitation character on the $^1\Pi_u$ states we carried out STEOM-CC, EOM-CC, and extended-STEOM-CCSD calculations using Sadlej's basis set[44,45] and additional diffuse functions in the center of the molecule. The calculations have been carried out at a bond distance of 2.069 bohr. In Table III it is seen that these three methods agree quite well for all dipole allowed states, except for the $b\ ^1\Pi_u$ state, which drops by 0.3 eV in the extended-STEOM calculations and which acquires substantial double excitation character, but only in this advanced calculation. There are no signs in the EOM-CC and STEOM calculations that the $b\ ^1\Pi_u$ state has a larger double excitation component and might be inaccurate therefore. The extended-STEOM method which has been shown to be about equally accurate for singly and doubly excited states[26] does capture this feature of the $b\ ^1\Pi_u$ state. The lowering of the excitation energy is clearly due to the admixture of considerable double excitation character. We also note that there is a substantial difference of 0.45 eV for the $c\ ^1\Pi_u$ state between our EOM-CC calculation in the large basis set and the earlier EOM-CC calculation.[10] Our present result are in better agreement with previous studies and with experiment.

TABLE III. Vertical excitation energies (in eV) from STEOM-CC, ext-STEOM-CC, and EOM-CC calculations for dipole-allowed transitions of N_2 in comparison to experimental values (Ref. 6).

Label	Expt. fit[a]	STEOM	Ext-STEOM	EOM-CC
$c\ ^1\Pi_u$	12.90	12.76	12.75	12.78
$b\ ^1\Pi_u$	13.24	13.55	13.24	13.57
$o\ ^1\Pi_u$	13.63	13.65	13.57	13.66
$c'\ ^1\Sigma_u^+$	12.98	12.78	12.79	12.83
$b'\ ^1\Sigma_u^+$	14.25	14.13	14.17	14.19
$e'\ ^1\Sigma_u^+$	14.48	14.42	14.55	14.62

[a]Reference 6.

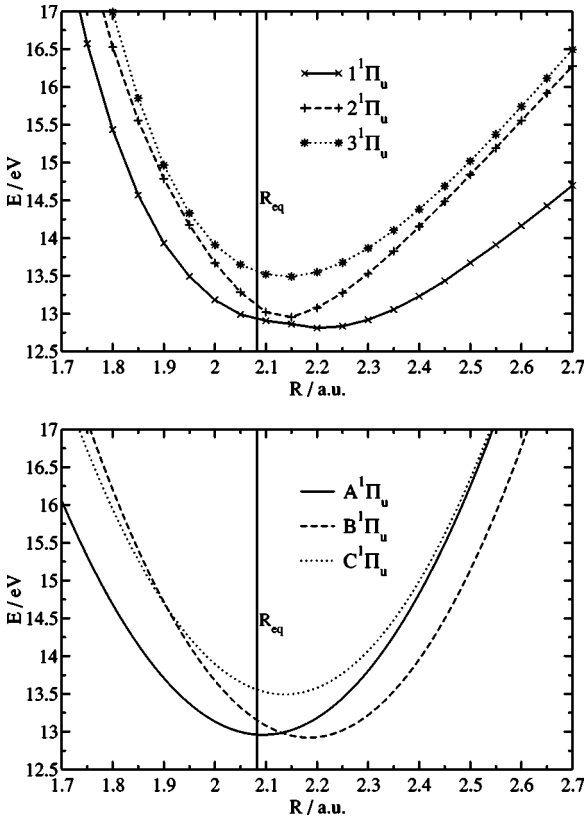

FIG. 2. Potential energy curves for the three lowest states of $^1\Pi_u$ symmetry. Top: calculated adiabatic potential energy curves. Bottom: diabatic model potential energy curves from Taylor expansion of diagonal elements of the effective Hamiltonian.

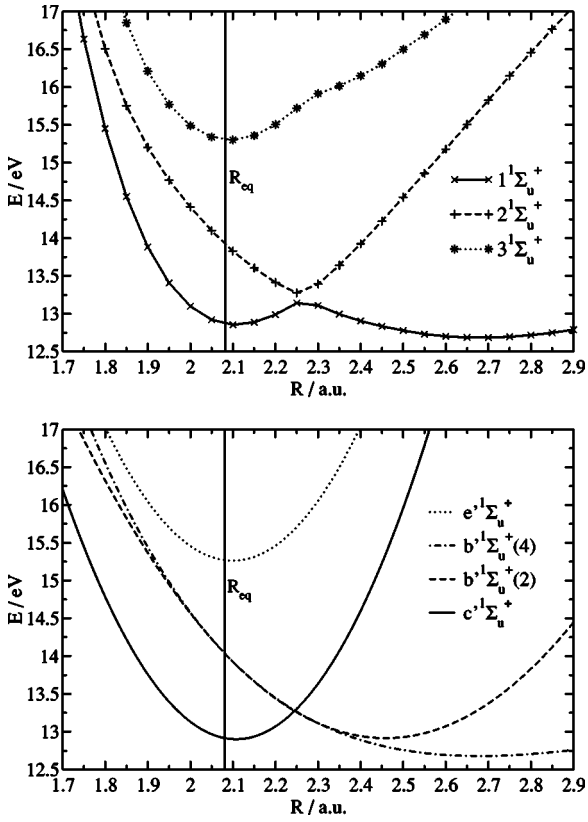

FIG. 3. Potential energy curves for the three lowest states of $^1\Sigma_u^+$ symmetry. Top: calculated adiabatic potential energy curves. Bottom: diabatic model potential energy curves from Taylor expansion of diagonal elements of the effective Hamiltonian. Two curves are given for the $b'\ ^1\Sigma_u^+$ state, namely, a quadratic (2) and a fourth-order model (4).

The results from the extended-STEOM calculation provide a strong indication that the experimental assignment is indeed correct.

The problem of the vibronic couplings between these states and the difficulties to obtain experimental ''vertical'' excitation energies clearly indicate that it is necessary to compare the full excited-state potential energy curves and include nonadiabatic effects in order to obtain a better understanding of the quality of TDDFRT/SAOP for the description of excited states of N_2.

IV. POTENTIAL ENERGY CURVES

We calculated potential energy curves of the three lowest states of both $^1\Sigma_u^+$ symmetry and $^1\Pi_u$ symmetry. The explicitly calculated adiabatic curves are shown in the upper parts of Figs. 2 and 3. To draw conclusions about avoided crossings and nonadiabatic couplings between these states, we constructed diabatic model potential energy curves from the Taylor expansion for the diagonal elements of the diabatic potential energy matrix according to the diabatizing scheme mentioned in Sec. II. We checked that the adiabatic model potential energy curves, which can be obtained by diagonalization of the diabatic potential energy matrix, resemble the explicitly calculated potential energy surfaces within the trust radius of the quadratic model. This validates the TDDFRT diabatizing scheme used to extract the coupling constants in the vibronic model. Since the totally symmetric normal mode in N_2 may not couple states of different symmetry, we treat each of the symmetries separately.

A. $^1\Pi_u$ states

For the $^1\Pi_u$ states, the diabatic model potential energy curves are shown in the lower part of Fig. 2. In order not to confuse the notation for adiabatic and diabatic states, the former will be denoted by numbers, while the latter are characterized by the capitals *A*, *B*, *C*. We do not adopt the experimental notation here since this would introduce an ambiguity due to the assignment problem for these states. The *A* state has orbital character $3\sigma_g \rightarrow 2\pi_u$ (Ry), the *B* state is the Rydberg state $1\pi_u \rightarrow 4\sigma_g$, and the *C* state is the valence excitation $2\sigma_u \rightarrow 1\pi_g$. The 1, 2 and 3 $^1\Pi_u$ states, respectively, have the same character at R_{eq}.

The diabatic model potential energy curves for the $^1\Pi_u$ states are close to the adiabatic states in a region around the equilibrium geometry (within the trust radius of the quadratic model), except for the fact that they show crossings where avoided crossings occur for the adiabatic states. The adiabatic curves, however, are much shallower for long bond distances, which cannot be reproduced by the second-order Taylor series expansion for the effective Hamiltonian. For the same reason, their increase towards short bond distances is steeper than in our quadratic model.

The $^1\Pi_u$ curves demonstrate the issue raised concerning

TABLE IV. Vibrational wave numbers (in cm^{-1}) of the diabatic excited states for dipole-allowed transitions of N_2 using the ET-QZ3P-3DIFFUSE basis set. Two types of frequencies have been extracted from the SAOP calculations: (a) the frequencies of the diabatic model potential energy surfaces (column "diab."); (b) second derivatives of the adiabatic excited-state energy curve (labeled with the numbers 1, 2, 3 as in the figures) at the positions of the diabatic states minima using a quadratic fit to five data points (column "adiab."). Experimental values (Refs. 1 and 2) and recommended harmonic wave numbers from Ref. 7 are given for comparison. For the experimental values, the vibrational spacings between the lowest vibrational states assigned in experiment are shown (i.e., the $(|0\rangle,|1\rangle)$ energy spacing in all cases except the $b'\,^1\Sigma_u^+$ state, where the $(|5\rangle,|6\rangle)$ spacing had to be taken).

Label	Excitation	MR-CI (+fit)[a]	Expt. Refs. 1 and 2	SAOP	
				Diab.	Adiab.
$b\,^1\Pi_u$	$2\sigma_u \rightarrow 1\pi_g$	681.1	605	*C*: 2483	3: 2188
$c\,^1\Pi_u$	$3\sigma_g \rightarrow 2\pi_u$	2228.2	2420	*A*: 2353	1: 2458
$o\,^1\Pi_u$	$1\pi_u \rightarrow 4\sigma_g$	1905.9	1976	*B*: 2449	2: 2108
$c'\,^1\Sigma_u^+$	$3\sigma_g \rightarrow 3\sigma_u$	2174.8	2016	c': 2347	1: 2285
$b'\,^1\Sigma_u^+$	$1\pi_u \rightarrow 1\pi_g$	746.2	686	b': 1476	2: 817
$e'\,^1\Sigma_u^+$	$3\sigma_g \rightarrow 4\sigma_u$	2216.2	⋯	e': 2336	3: 2336

[a]Reference 7.

the assignment. The TDDFRT/SAOP calculations (here and in Ref. 13) result in $3\sigma_g \rightarrow 2\pi_u$ Rydberg character for the lowest diabatic $^1\Pi_u$ state ($A\,^1\Pi_u$) at R_{eq}, and $1\pi_u \rightarrow 4\sigma_g$ Rydberg character for the second lowest ($B\,^1\Pi_u$). The valence excitation $2\sigma_u \rightarrow 1\pi_g$ appears in the highest of these three $^1\Pi_u$ states ($C\,^1\Pi_u$). However, experimentally the second excited $^1\Pi_u$ state at R_{eq}, ($b\,^1\Pi_u$, see Fig. 1), has been assigned this valence excitation character, on the basis of the low vibrational frequencies of 600–700 cm^{-1} (cf. the frequencies in Table IV). Strong change from the ground-state frequency is usually indicative of valence character of an excitation. We note that in the SAOP calculation, the $2\sigma_u \rightarrow 1\pi_g$ valence excitation does not show a low frequency, as can also be seen qualitatively from the $C\,^1\Pi_u$ curve in Fig. 2. The vibrational frequency of this $C\,^1\Pi_u$ state is 2483 cm^{-1} and therefore, similar to the calculated harmonic ground-state vibrational frequency of 2349 cm^{-1}. Actually, this excitation is from an antibonding to an antibonding orbital, and its valence character need not automatically imply that the vibrational frequency will be much lower than the ground-state frequency. This argument for the assignment of the valence $2\sigma_u \rightarrow 1\pi_g$ character to the low-frequency $b\,^1\Pi_u$ is therefore not valid.

The adiabatic $3\,^1\Pi_u$ state corresponds to the diabatic $C\,^1\Pi_u$ over the R range considered. If this curve would be assigned to the experimentally highest lying $o\,^1\Pi_u$, the experimental low frequency of the state with the lowest minimum ($b\,^1\Pi_u$) has to be explained by vibronic coupling between the $A\,^1\Pi_u$ and $B\,^1\Pi_u$, which individually have high frequencies, cf. Table IV. This nonadiabatic effect results in a softening of the potential, see the adiabatic $1\,^1\Pi_u$ curve. We will in the following section falsify this conjecture by explicitly considering nonadiabatic effects through a diabatizing scheme.

It is instructive at this point to make a comparison to the work by Spelsberg and Meyer,[7] who in 2001 reported adiabatic and diabatic potential energy curves for the three lowest states of $^1\Pi_u$ and $^1\Sigma_u^+$ symmetry from MR-CI calculations. Their diabatic potentials, given in Fig. 1, appear to match the experimental findings. Clearly, the diabatic states are not uniquely defined, but since they qualitatively serve the same purpose to avoid sudden changes in the character of the excited states, and since far away from avoided crossings they should be similar to the adiabatic curves, comparison to our diabatic curves around R_e and to the adiabatic ones further from R_e, should be meaningful.

A main difference between the *adiabatic potentials* is that the $1\,^1\Pi_u$ state from the TDDFRT/SAOP calculations has a different orbital character for large bond distances. According to the MR-CI calculation from Ref. 7, this state changes its character from a $3\sigma_g \rightarrow 2\pi_u$ Rydberg state for bond distances up to ≈2.1 bohr to a $2\sigma_u \rightarrow 1\pi_g$ valence state at longer bond distances, due to a crossing of the diabatic $c\,^1\Pi_u$ and $b\,^1\Pi_u$ states.

The Rydberg $3\sigma_g \rightarrow 2\pi_u$ character at short bond distance agrees with the character of our $1\,^1\Pi_u$ adiabatic state for $R < 2.1$ bohr, but for larger distances we again obtain Rydberg character, now of $1\pi_u \rightarrow 4\sigma_g$ nature.

The MR-CI calculations reveal a further significant difference with the TDDFRT calculations. In the MR-CI calculations very soon (over the distance range 2.0–3.0 bohr) the $2\sigma_u \rightarrow 1\pi_g$ valence excitation character is replaced with double excitation character, the valence double excitation $3\sigma_g$, $1\pi_u \rightarrow (1\pi_g)^2$. Such a double excitation cannot be represented with the TDDFRT. This observation suggests that the discrepancy between the TDDFRT calculations and experiment should not be reconciled by a reassignment of the orbital transitions to the experimental states but must be attributed to a too high energy of the TDDFRT valence excited state (the diabatic $C\,^1\Pi_u$ and adiabatic $3\,^1\Pi_u$) caused by lack of double excitation character.

In this case our Rydberg diabatic states $A\,^1\Pi_u$ and $B\,^1\Pi_u$ should correspond to the MR-CI diabatic $c\,^1\Pi_u$ and $o\,^1\Pi_u$ states. The $3\sigma_g \rightarrow 2\pi_u$ Rydberg excited state (denoted $c\,^1\Pi_u$ in Fig. 1 and $A\,^1\Pi_u$ in Fig. 2) has its minimum position at 2.1 bohr in both calculations, and the minimum of the Rydberg $1\pi_u \rightarrow 4\sigma_g$ state ($o\,^1\Pi_u$ in Fig. 1 and $B\,^1\Pi_u$ in Fig. 2) is at ≈2.18 bohr for SAOP and 2.20 bohr for MR-CI. The vibrational frequencies for the *c*, *A* state are quite similar (2353 cm^{-1} for SAOP, 2228.2 for MR-CI), while they are

TABLE V. Excited state energies (in eV) from accurate Kohn–Sham potentials based on *ab initio* densities of N_2 near the ground-state equilibrium (2.074 bohr) and at 2.5 bohr. SAOP results are shown for comparison. All values are given w.r.t. the ground-state energy at 2.074 bohr.

	$R=2.074$ bohr		$R=2.500$ bohr	
Transition	Accurate KS	SAOP	Accurate KS	SAOP
$3\sigma_g \rightarrow 2\pi_u$	13.10	12.92	15.06	14.82
$1\pi_u \rightarrow 4\sigma_g$	13.22	13.17	13.63	13.67
$2\sigma_u \rightarrow 1\pi_g$	13.78	13.58	15.17	15.01

somewhat higher for SAOP in case of the *o*, *B* state (2449 cm^{-1} compared to 1905.9 for MR-CI). This is due to our approximation of second-order Taylor expansion at the ground state R_{eq}, the frequency of the adiabatic curve evaluated at the excited state R_{eq} being with 2108 cm^{-1} close to the experimental 1976 cm^{-1}. So there is actually good agreement for these Rydberg potential energy curves, although $B\,^1\Pi_u$ is somewhat vertically shifted in case of the SAOP potential: While the vertical position of the $A\,^1\Pi_u$ minimum coincides with the $c\,^1\Pi_u$ MR-CI curve within ≈0.1 eV, the $B\,^1\Pi_u$ state is about 0.3 eV too low in energy compared to the $o\,^1\Pi_u$ MR-CI results.

The valence excited state $C\,^1\Pi_u$ has definitely wrong energy and shape. It should correspond to the $b\,^1\Pi_u$ state, and thus have a shallow minimum at much larger bond length (≈2.45 bohr) at lower energy than the *A*, $B\,^1\Pi_u$ minima (the $b\,^1\Pi_u$ minimum is ≈0.4 eV below the minimum energy of the $c\,^1\Pi_u$ state, cf. Fig. 1). Instead of this, SAOP yields a minimum at 2.15 bohr for this state, at about 0.6 eV higher energy than the minimum energy of the $C\,^1\Pi_u$ state.

These differences between the MR-CI calculations and our TDDFRT calculations cannot be explained by the approximate nature of the exchange-correlation potential, as may already be inferred from the fact that *all* exchange-correlation potentials investigated in Refs. 13 and 12 place the $2\sigma_u \rightarrow 1\pi_g$ higher in energy than the other two $^1\Pi_u$ vertical excitation energies. As a definite proof for this assertion, we calculated the excitation energies using an accurate Kohn–Sham (KS) potential constructed from densities obtained in sophisticated MR-CI calculations using Dunning's aug-cc-pVQZ basis set.[46,47] The KS solution was obtained using the iterative local updating scheme of van Leeuwen and Baerends.[48] Calculations of excited-state energies have been performed for structures with bond distances near the ground-state equilibrium (2.074 bohr, which corresponds to the distance used in Ref. 49) and at 2.5 bohr. The orbital energies of the former calculation have been checked against those of earlier work[49] and are in excellent agreement. The results are shown in Table V together with SAOP data using exactly the same structures and integration grids. It can be seen that the excited-state energies from SAOP and potentials based on highly accurate *ab initio* densities agree in all cases investigated here within 0.24 eV. The energy for the $2\sigma_u \rightarrow 1\pi_g$ transition at 2.5 bohr is about 15.2 eV higher than the ground-state minimum energy, while the MR-CI value is ≈12.6 eV. The qualitative differences between TDDFRT and MR-CI calculations at long distances are thus also obtained with very accurate KS potentials.

B. $^1\Sigma_u^+$ states

The $^1\Sigma_u^+$ excited states do not offer such problems as the $^1\Pi_u$ states do. Considering first the adiabatic curves, we note that there is qualitative agreement of the lowest adiabatic $^1\Sigma_u^+$ states to experiment and MR-CI calculations, regarding their shape and minimum position. We emphasize that the TDDFRT calculations apparently have no problem in describing the avoided crossing: the bond distance of the avoided crossing between the two lowest states is only slightly smaller in the SAOP calculation (2.25 bohr compared to 2.3 for MR-CI), and the minimum positions of the $1\,^1\Sigma_u^+$ state (2.1 for both SAOP and MR-CI) are approximately the same. There is a second minimum of the adiabatic $1\,^1\Sigma_u^+$ state, due to the coupling with the $2\,^1\Sigma_u^+$ state, in a very flat potential energy well at ≈2.7 bohr in both the SAOP and MR-CI calculations. Also the minimum positions of the $3\,^1\Sigma_u^+$ states are close (2.1 for SAOP, 2.15 for MR-CI), but as has already been pointed out in Sec. III, this Rydberg state is too high in energy. The additional nonadiabatic coupling at a bond distance of about 2.3 bohr, which can be recognized for this state (SAOP) is not present in the MR-CI case. But since this coupling to higher-lying states is maybe artificial, being induced by the high vertical excitation energy for this state, and since the $3\,^1\Sigma_u^+$ state has a rather low transition moment and therefore will not significantly influence the spectra simulation anyway, we omit the influence of higher $^1\Sigma_u^+$ states on the $3\,^1\Sigma_u^+$ in our simulation. We would like to note that this state is quite sensitive to the exchange-correlation potential employed in the calculation, as was observed in calculations using, e.g., accurate Kohn–Sham potentials as mentioned above. They indeed lead to much lower excitation energies, which indicates a deficiency of the SAOP potential to be a possible error source for this particular state.

The diabatic $^1\Sigma_u^+$ curves are shown in Fig. 3. Since there is not an assignment issue here, we simply adopt the notation used in the experimental and MR-CI work. There is a crossing of the diabatic $c'\,^1\Sigma_u^+$ and $b'\,^1\Sigma_u^+$ states at a bond distance of 2.25 bohr, which corresponds to the avoided crossing of the adiabatic $1\,^1\Sigma_u^+$ and $2\,^1\Sigma_u^+$ states. Again, far away from the equilibrium distance the diabatic curves do not resemble the adiabatic curves, but this is primarily due to our quadratic model that only uses the shape of the curve at R_{eq} as input. In particular the minimum position of $b'\,^1\Sigma_u^+$ seems to be at too short bond distances (about 2.45 bohr) compared to the adiabatic curve, which has a minimum at very long distance, ≈2.7 bohr. Nevertheless, the frequency of the $b'\,^1\Sigma_u^+$ diabatic state is, with 1476 cm^{-1}, much lower than those of the other excited states, although not as low as the 686 cm^{-1} in the experiment (see Table IV).

The second derivative, evaluated at the minimum of the adiabatic curve, which could be located at 2.68 bohr by additional calculations, is 817 cm^{-1} in very good agreement with the MR-CI value (values between 745 and 856 cm^{-1} were obtained for different reasonable step sizes, reflecting

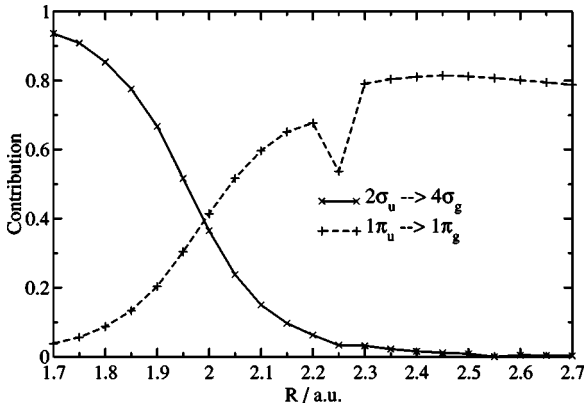

FIG. 4. Contributions of the $2\sigma_u \rightarrow 4\sigma_g$ and $1\pi_u \rightarrow 1\pi_g$ singly excited configurations to the adiabatic excited states with the character of the valence $b'\,^1\Sigma_u^+$ state at the ground-state equilibrium.

the large anharmonic contributions for this curve). The MR-CI diabatic curves follow the adiabatic curves at distances where there is little or no nonadiabatic coupling. This is due to the different diabatizing schemes. Spelsberg and Meyer[7] apply r^2 matrix elements to find the transformation matrix between adiabatic and diabatic states along the full potential energy curve in the range of interest. This leads to a $b'\,^1\Sigma_u^+$ state for which two configurations are important, whose contributions vary smoothly along the normal coordinate. The approach used in our work employs the region near the *ground-state equilibrium*, and tries to preserve the character of the excited states there within a second-order Taylor series expansion.

The two important configurations for the $b'\,^1\Sigma_u^+$ state are—in contrast to the $b\,^1\Pi_u$ state—both singly excited. The TDDFRT calculations can handle this situation, and the adiabatic $1\,^1\Sigma_u^+$ curve has a correct behavior at longer distance (around 2.7 bohr). Figure 4 shows the corresponding contributions of the $2\sigma_u \rightarrow 4\sigma_g$ and the $1\pi_u \rightarrow 1\pi_g$ excited configurations in our SAOP calculations. These contributions are obtained from those *adiabatic* excited states which have the largest overlap with the $2\,^1\Sigma_u^+$ state at R_{eq} (i.e., the adiabatic state which is closest to the diabatic $b'\,^1\Sigma_u^+$ state at a certain geometry). As can be seen from this figure this state is dominated by the $2\sigma_u \rightarrow 4\sigma_g$ transition for short bond distances, while for distances larger than ≈ 2 bohr the $1\pi_u \rightarrow 1\pi_g$ excited configuration becomes more important. The nonadiabatic coupling between the two lowest excited $^1\Sigma_u^+$ states at a distance of 2.2–2.3 bohr is reflected in the curve of Fig. 4 by discontinuities. This picture is very similar to the analysis of the configuration classes in Ref. 7.

It becomes clear that a low-order Taylor series expansion for this state is not well suited to reproduce the experimental findings. To improve on the quadratic potential we used a quartic polynomial for the diabatic $b'\,^1\Sigma_u^+$ state energy (i.e., only for the diagonal contribution of this state to the potential energy matrix), which should be more adequate to model the long-range behavior of the adiabatic $1\,^1\Sigma_u^+$ state. Because of the smooth change in the important configurations for this diabatic state (cf. Fig. 4), the third and fourth derivatives of the diabatic excited-state energy at R_{eq} do not lead to a correct shape of the potential in the region around the outer $1\,^1\Sigma_u^+$ state minimum. Furthermore, these terms introduce unbound potentials in the model Hamiltonian, so that no converged results in the spectrum simulation can be expected. We solved this problem by constructing a fourth-order expansion with the following constraints:

(i) The vertical excitation energy and its first derivative are fixed to the values obtained from the second-order expansion presented above.

(ii) The position of the excited-state minimum was fixed to the bond distance and energy of the adiabatic $1\,^1\Sigma_u^+$ state minimum.

(iii) The energy for a very large bond distance was also fixed to the value of the adiabatic $1\,^1\Sigma_u^+$ state at that position (3.5 bohr/13.71 eV; well separated from other electronic states in this region) to ensure a bound potential, i.e., a positive coefficient for the fourth-order term.

The potential energy curve for this model, $b'\,^1\Sigma_u^+(4)$, is shown in Fig. 3. A comparison with the adiabatic curves demonstrates that at both long and short bond distances this curve leads to a large improvement of the excited-state model potential compared to $b'\,^1\Sigma_u^+(2)$.

Comparing finally the diabatic Rydberg states $c'\,^1\Sigma_u^+$ and $e'\,^1\Sigma_u^+$ from SAOP and MR-CI calculations, we observe that they show the same minimum position (between 2.10 and 2.15 bohr for both states in both calculations), and there is also qualitative agreement in the high vibrational frequencies for these states (considering the neglect of anharmonic and empirical corrections in our study), see Table IV.

V. VIBRONICALLY COUPLED SPECTRA

In order to simulate the fine structure of the spectra, we used the second-order expansion of the diabatic potential energy matrix from the SAOP/ET-QZ3P-3DIFFUSE calculation. We performed the analysis of the $^1\Sigma_u^+$ and $^1\Pi_u^+$ states separately in order to distinguish their contributions to the spectra.

The vibronic excitation energies were obtained in the direct-product basis of the three electronic $^1\Sigma_u^+$ or $^1\Pi_u^+$ states, respectively, and up to 160 vibrational quanta in the bond stretching mode for the nuclear part. In the quartic model, up to 400 vibrational quanta have been used to converge also the position of the highest vibrational states in the $b'\,^1\Sigma_u^+$ absorption band, while the states up to $\approx v=15$ are already converged with a much lower number of quanta. The large number of necessary quanta reflects the fact that excited-state vibrational wave functions are modeled by linear combinations of ground-state harmonic oscillator wave functions. Lorentz–Profile spectra with a line width of 0.015 eV are depicted in Fig. 5. The peak positions and the assignment to vibronic transitions are shown in Tables VI (for $^1\Sigma_u^+$) and VII (for $^1\Pi_u$). The assignments are based on the energy differences to the $|0\rangle \rightarrow |0\rangle$ transitions and the analysis of the Lanczos eigenvectors obtained from the VIBRON package.[43] Note that due to the nonadiabatic effects some levels may have important contributions from several electronic times vibrational basis states.

We can see from the upper diagram in Fig. 5 that the

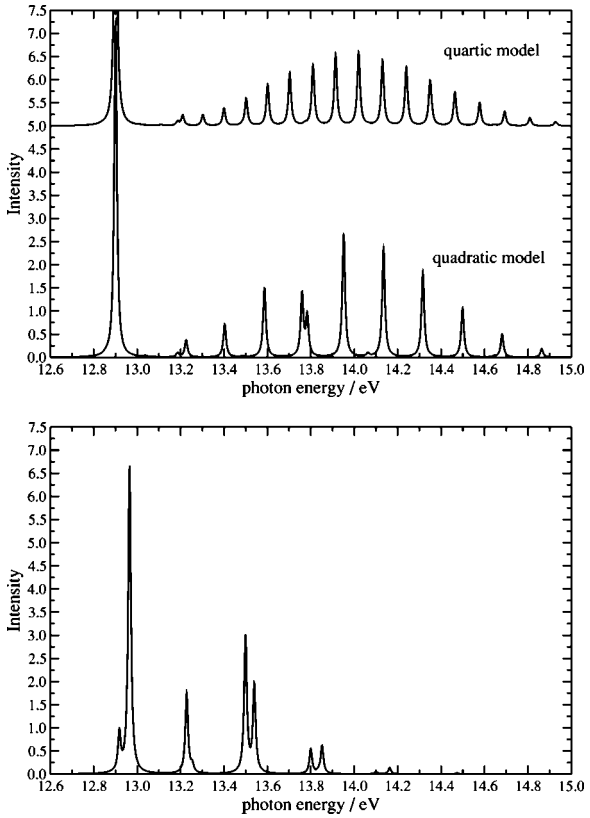

FIG. 5. Electronic absorption spectra obtained from the second-order Taylor expansion of the potential energy matrix **V**(q), Eq. (1), in a vibronic coupling simulation. Top: contribution of the $^1\Sigma_u^+$ states using a quadratic or quartic model, respectively, for the $b'\,^1\Sigma_u^+$ state. Bottom: contribution of the $^1\Pi_u^+$ states.

TABLE VI. Main contributions (diabatic electronic states and excited-state vibrational levels v), excitation energies (eV), and oscillator strengths to the vibronic transitions for $^1\Sigma_u^+$ states of N_2 from SAOP/ET-QZ3P-3DIFFUSE calculations. Experimental values are given for comparison in those cases, where one particular configuration dominates. Note that the fourth-order expansion was applied to model the $b'\,^1\Sigma_u^+$ state.

Main contribution		SAOP		Expt.[a]	
Electronic state	v	Energy (eV)	f	Energy (eV)	f
$c'\,^1\Sigma_u^+$	0	12.900	0.2165	$c'\,^1\Sigma_u^+$: 12.935	0.195
$c'\,^1\Sigma_u^+$	1	13.187	0.0027	$c'\,^1\Sigma_u^+$: 13.185	0.001 47
$c'\,^1\Sigma_u^+$	1	13.210	0.0069		
and $b'\,^1\Sigma_u^+$	6			$b'\,^1\Sigma_u^+$: 13.390	0.002 16
$b'\,^1\Sigma_u^+$	7	13.303	0.0072	⋯	⋯
$b'\,^1\Sigma_u^+$	8	13.400	0.0117	⋯	⋯
$c'\,^1\Sigma_u^+$	2	13.502	0.0185	$c'\,^1\Sigma_u^+$: 13.475	0.0155
and $b'\,^1\Sigma_u^+$	9			$b'\,^1\Sigma_u^+$: 13.660	0.0128
$b'\,^1\Sigma_u^+$	10	13.601	0.0276	$b'\,^1\Sigma_u^+$: 13.760	0.002 20
$b'\,^1\Sigma_u^+$	11	13.703	0.0358	$b'\,^1\Sigma_u^+$: 13.830	0.006 54
$b'\,^1\Sigma_u^+$	12	13.810	0.0412	$b'\,^1\Sigma_u^+$: 13.910	0.0303
and $c'\,^1\Sigma_u^+$	3				
$b'\,^1\Sigma_u^+$	13	13.914	0.0491	$b'\,^1\Sigma_u^+$: 13.998	⋯
$b'\,^1\Sigma_u^+$	14	14.020	0.0512	$b'\,^1\Sigma_u^+$: 14.070	0.0341
$b'\,^1\Sigma_u^+$	15	14.130	0.0457	$b'\,^1\Sigma_u^+$: 14.150	0.0409
and $c'\,^1\Sigma_u^+$	4			$c'\,^1\Sigma_u^+$: 13.990	0.002 10
$b'\,^1\Sigma_u^+$	16	14.240	0.0413	$b'\,^1\Sigma_u^+$: 14.230	0.0626
$b'\,^1\Sigma_u^+$	17	14.349	0.0304	$b'\,^1\Sigma_u^+$: 14.300	0.0318
and $c'\,^1\Sigma_u^+$	5				
$c'\,^1\Sigma_u^+$	5	14.356	0.0040	$c'\,^1\Sigma_u^+$: 14.230	⋯
and $b'\,^1\Sigma_u^+$	17				
$b'\,^1\Sigma_u^+$	18	14.464	0.0243	$b'\,^1\Sigma_u^+$: 14.400	0.003 26
$b'\,^1\Sigma_u^+$	19	14.578	0.0168	$b'\,^1\Sigma_u^+$: 14.465	0.0166
$b'\,^1\Sigma_u^+$	20	14.693	0.0104	$b'\,^1\Sigma_u^+$: 14.525	0.0173
$b'\,^1\Sigma_u^+$	21	14.809	0.0060	⋯	⋯
$b'\,^1\Sigma_u^+$	22	14.927	0.0029	$b'\,^1\Sigma_u^+$: 14.680	0.004 55
and $c'\,^1\Sigma_u^+$	7				
$b'\,^1\Sigma_u^+$	23	15.046	0.0015	$b'\,^1\Sigma_u^+$: 14.737	0.008 97
$e'\,^1\Sigma_u^+$	0	15.262	0.0041	$e'\,^1\Sigma_u^+$: 14.350	0.0104

[a]Reference 1.

overall picture of the contributions of the $^1\Sigma_u^+$ states to the total vibronic spectrum is, in both the quadratic and the quartic models, in qualitative agreement with the deconvolution of peaks in Ref. 1. There is only one very strong vibronic peak, at 12.901 eV (experimentally 12.935), arising from the $c'\,^1\Sigma_u^+$ state, as can be expected for potential energy curves which are only vertically displaced from the equilibrium structure. Also the $v=1$ state (the low intensity peak of the doublet at ≈13.2 eV) has been discerned in the experiment. The $b'\,^1\Sigma_u^+$ state on the other hand shows a pronounced vibrational progression, corresponding to its considerably displaced R_{eq}, with maximum intensity around 14.0 eV (maximum intensity in experiment: 14.23 eV), which suggests that the vertical excitation energy for this state is in good agreement with experiment. There is a clear difference in the quadratic and the quartic models with respect to the vibrational spacings, the ≈800 cm^{-1} of the quartic model being in much better agreement with experiment (686 cm^{-1}) than the value of 1476 cm^{-1} obtained in the quadratic model. The slight increase in the vibrational spacing for the higher vibrational levels in the $b'\,^1\Sigma_u^+$ band are caused by the dominant quartic contribution to the potential for these quantum numbers. In the quadratic model, there is a deviation from a normal Franck–Condon type intensity pattern at about 13.8 eV due to the coupling with the $c'\,^1\Sigma_u^+$ state, which can also be recognized in the experimental data. Due to the change in peak positions in the quartic model, this feature of an ''intensity stealing'' by the $v=3$ level of the $c'\,^1\Sigma_u^+$ state disappears. It indicates how sensitive the modeling of couplings between the different states is even to slight shifts (smaller than 0.1 eV) in the energy of the vibronic levels, since the couplings between these two electronic states are quite small. Altogether we can conclude that the modeling of the vibronic spectrum of the $^1\Sigma_u^+$ states is satisfactory in view of the approximate nature of the diabatizing scheme employed in this work, and demonstrates the reliability of the TDDFRT/SAOP calculations for this purpose.

Turning now to the $^1\Pi_u$ states, we recall that the experimental spectrum shows a progression of vibronic bands (the Birge–Hopfield bands) starting at 12.500 eV, with a spacing of ≈0.075 eV (605 cm^{-1}), with the maximum at the $v=4$ level at 12.835 eV. For higher energies, the bands of decreasing intensity of this progression, which have been attributed to the valence $b\,^1\Pi_u$ state, become masked by the strong $v=0$ band of the $c'\,^1\Sigma_u^+$ band at 12.935 we have just discussed. It is evident from Fig. 5 and Table VII that such a regular vibrational progression with low frequency does not result from coupling of the $A\,^1\Pi_u$ and $B\,^1\Pi_u$ states. We clearly see a typical Franck–Condon vibrational progression

TABLE VII. Main contributions (diabatic electronic states and excited-state vibrational levels v), excitation energies (eV), and oscillator strengths to the vibronic transitions for $^1\Pi_u$ states of N_2 from SAOP/ET-QZ3P-3DIFFUSE calculations. Experimental values are given for comparison.

Main contribution		SAOP		Expt.[1]	
Electronic state	v	Energy (eV)	f	Energy (eV)	f
$B\,^1\Pi_u$	0	12.918	0.0246	$o\,^1\Pi_u$: 13.100	⋯
and $A\,^1\Pi_u$	0				
$A\,^1\Pi_u$	0	12.965	0.1988	$c\,^1\Pi_u$: 12.910	0.0635
$B\,^1\Pi_u$	1	13.228	0.0529	$o\,^1\Pi_u$: 13.345	0.0211
and $A\,^1\Pi_u$	1				
$A\,^1\Pi_u$	1	13.254	0.0050	$c\,^1\Pi_u$: 13.210	0.0640
$C\,^1\Pi_u$	0	13.499	0.0920	$b\,^1\Pi_u$: 12.500	0.002 54
$B\,^1\Pi_u$	2	13.539	0.0576	$o\,^1\Pi_u$: 13.585	0.0277
$A\,^1\Pi_u$	2	13.545	0.0014	$c\,^1\Pi_u$: 13.475	0.0155
$C\,^1\Pi_u$	1	13.800	0.0170	$b\,^1\Pi_u$: 12.575	0.0113
$A\,^1\Pi_u$	3	13.835	0.0013	⋯	⋯
$B\,^1\Pi_u$	3	13.852	0.0193	$o\,^1\Pi_u$: 13.820	0.0236
and $A\,^1\Pi_u$	3				
and $C\,^1\Pi_u$	1				
$C\,^1\Pi_u$	2	14.100	0.0018	$b\,^1\Pi_u$: 12.663	0.0272
and $B\,^1\Pi_u$	4				
$B\,^1\Pi_u$	4	14.163	0.0044	$o\,^1\Pi_u$: 14.050	0.006 20
and $C\,^1\Pi_u$	2				

corresponding to the displaced $B\,^1\Pi_u$ diabatic state, starting at 12.92 eV with a low intensity peak, with subsequent peaks at 13.23, 13.54 (maximum), 13.85, and 14.16, with spacing of 0.31 eV. This state is slightly too low, the experimental $|0\rangle\rightarrow|0\rangle$ transition (not identified in the spectrum) has been inferred to be ≈0.2 eV higher. The $A\,^1\Pi_u$ state shows a high intensity only for the $|0\rangle\rightarrow|0\rangle$ transition at 12.97 eV in our calculation, while the intensity rapidly goes down for higher final vibrational states, since the potential energy curve is almost only vertically shifted compared to the ground state. Already the $v=1$ peak at 13.25 eV, just to the right of the second $B\,^1\Pi_u$ state, is barely visible. The coupling between the $B\,^1\Pi_u$ and $A\,^1\Pi_u$ diabatic states hardly shows up in the calculated vibronic spectrum. Evidently, such coupling cannot be invoked to explain the low energy vibrational progression in the experimental spectrum. We therefore conclude that the $A\,^1\Pi_u$ and $B\,^1\Pi_u$ diabatic Rydberg states should be associated with the experimental $c\,^1\Pi_u$ and $o\,^1\Pi_u$ states, respectively, not with the $b\,^1\Pi_u$ state. Their $|0\rangle\rightarrow|0\rangle$ transition energies are indeed in very good agreement with the experimental $c\,^1\Pi_u$ and $o\,^1\Pi_u$ ones, see Table VII. The intensities of the vibrational progressions are somewhat harder to compare, since the experimental vibrational progressions are strongly overlapping. The vibrational spacing of $B\,^1\Pi_u$ (2449 cm^{-1}) is somewhat too high compared to the experimental $o\,^1\Pi_u$ progression (1976 cm^{-1}), which however would be improved considerably when the second derivative of the adiabatic $1\,^1\Pi_u$ curve would be taken at the position of the minimum (2108 cm^{-1}). The slightly high frequency is therefore due primarily to our second-order Taylor series approximation around the ground state R_{eq}. We observe that transitions involving higher vibrational levels of this state still have considerable intensities, as is the case in the experiment for $o\,^1\Pi_u$. For the $c\,^1\Pi_u$ state the vibrational spacing agrees well with that computed for the $A\,^1\Pi_u$ state. The intensity distribution is slightly different in experiment, according to the deconvolution of Ref. 1. Instead of the strong $|0\rangle\rightarrow|0\rangle$ and weak $|0\rangle\rightarrow|1\rangle$ peaks in our calculation, these transitions show similar intensities for $c\,^1\Pi_u$. This could be related to a slightly wrong minimum position of the SAOP $A\,^1\Pi_u$ potential curve.

The conclusion has to be that the valence excited diabatic $C\,^1\Pi_u$ state, in spite of the energy mismatch, has to be associated with the experimental lowest excited state $b\,^1\Pi_u$. The first transitions involving mainly vibrational levels of the $C\,^1\Pi_u$ can clearly be identified in our calculation. As expected, the energy for the $|0\rangle\rightarrow|0\rangle$ transition is much too high (13.499 eV for SAOP, 12.500 for $b\,^1\Pi_u$ in the experiment). The discrepancy for the $|0\rangle\rightarrow|1\rangle$ transition is even larger (13.800 for SAOP compared to 12.575 in experiment). This reflects the wrong shape and the much too high vibrational frequency found for the diabatic potential energy curve in the SAOP calculation. We can infer from the configuration analysis in Ref. 7 that the relatively low energy and shallow nature of the $b\,^1\Pi_u$ state is apparently due to the admixing of the double excitation $3\sigma_g,\ 1\pi_u\rightarrow 1\pi_g^2$, which increases at longer bond lengths, becoming dominant beyond $R=2.4$ bohr. The $^1\Pi_u$ states therefore demonstrate that the states that can be described with single excitations, such as the Rydberg states $c\,^1\Pi_u$ and $o\,^1\Pi_u$, are given quite accurately by the TDDFRT/SAOP calculations, with indeed is a deviation for the $|0\rangle\rightarrow|0\rangle$ transition in the order of 0.1 eV, and with qualitatively correct frequencies. On the other hand, the state with considerable double excitation character $b\,^1\Pi_u$ is exhibiting a relatively large error of about 1 eV for the $|0\rangle\rightarrow|0\rangle$ transition.

VI. CONCLUSION

Our conclusions are twofold: First, our vibronic coupling calculations show that the shapes of the adiabatic potential energy curves of the TDDFRT/SAOP calculations, including the regions of avoided crossings, are in general quite satisfactory, apart from the one exception that is the key subject of this paper, see below. We have constructed diabatic model potential energy surfaces in terms of a Taylor series expansion of a diabatic potential energy matrix. We observe that remaining differences between the diabatic states calculated here and those from high-level MR-CI calculations are due to slight vertical shifts in the diabatic potential energy curves, leading to slightly different positions of avoided crossings in the adiabatic representation, and, more importantly, to the limited trust radius of the truncated Taylor-series expansion. Further improvement can be expected from including higher order terms in the Taylor-series expansion of the diabatic potential energy matrix, which can also account for anharmonicity effects in the excited-state potentials. However, higher-order terms may also lead to unbound potentials, making the simulation of spectra again very difficult. We have in the present work in an individual case improved on the second-order approximation at the ground state R_{eq} by applying a fourth-order approximation which also uses information about the long-range behavior of the excited state. Although the model employed here is too sim-

plistic to aim at a full quantitative reproduction of all experimentally known vibronic transitions, our present approximate second-order diabatic model Hamiltonian allows us to reproduce important features of the vibronic structure of the N_2 absorption spectrum. Especially the results for the contributions of the $^1\Sigma_u^+$ states, and of the singly excited (Rydberg) $^1\Pi_u$ states, show that SAOP calculations in combination with the simple TDDFRT diabatizing scheme employed in this study presents a promising way to the qualitative simulation of the vibronic structure of larger molecules, where the real power of the TDDFRT approach lies.

The important exception referred to earlier, involves a state with partially doubly excited character, which cannot be described in a linear-response TDDFT framework. The results for this $^1\Pi_u$ state demonstrate that the lack of any contribution of the double excitation $3\sigma_g$, $1\pi_u \rightarrow (1\pi_g)^2$ in the TDDFRT precludes the accurate description of the $b\,^1\Pi_u$. We could rule out, with the calculations performed in this work, the alternative assignment of orbital transitions to the experimentally measured absorption spectra, which as noted in Ref. 13 could ''save'' the good agreement of TDDFRT/SAOP calculations with experiment. In particular, it cannot be maintained that the vibrational progressions starting at 12.500 eV, with low energy spacings, could be caused by the nonadiabatic coupling of the two $^1\Pi_u$ Rydberg states. This means that the assignment of vertical SAOP excitation energies to experimental ones has to be the one shown in Table I, which also means that the excitation energy of the state with important double excitation character, the adiabatic $3\,^1\Pi_u$ (diabatic $C\,^1\Pi_u$), is significantly ($\approx$1 eV for the $|0\rangle \rightarrow |0\rangle$ transition, see Table VII) in error. This signals an important limitation of the current linear response based on TDDFT calculations of excitation energies.

There are several known examples, like the CN or CO^+ radicals,[50] linear polyene oligomers,[51] or unsaturated organic compounds like tetrazine[52] for which states with partly doubly excited character are apparently described correctly. In contrast to this our conclusion is that the wrong shape of the $b\,^1\Pi_u$ state is clearly caused by the inability of linear response TDDFT calculations to deal with doubly excited configurations; it cannot be attributed to the approximate nature of the exchange-correlation potential. This was shown by calculations with accurate Kohn–Sham potentials based on *ab initio* densities, which confirmed the accuracy of the SAOP potential and did not lead to any improvement in our case. As has been pointed out in Ref. 7 and confirmed by our (ST)EOM-CC calculations, also other single excitation based *ab initio* methods have problems with the $b\,^1\Pi_u$ state because of its doubly excited character, which explains that all these methods, like linear response TDDFT, yield a wrong description of this state. The extended-STEOM-CC approach, however, which is capable to describe doubly excited configurations, leads to significantly better results.

It is clear that proper incorporation of double excitations in TDDFRT is a major challenge for the near future. Recently, Maitra *et al.*[53] made an important step, proposing an adaptation of the exchange-correlation kernel, which introduces special frequency dependence of the kernel in cases where singly and doubly excited configurations mix. A routinely applicable procedure would obviously be highly desirable.

ACKNOWLEDGMENT

We are grateful to Dr. O. V. Gritsenko for providing us with the accurate Kohn–Sham potentials based on MR-CI densities.

[1] W. F. Chan, G. Cooper, R. N. S. Sodhi, and C. E. Brion, Chem. Phys. **170**, 81 (1993).
[2] J. Geiger and B. Schröder, J. Chem. Phys. **50**, 7 (1969).
[3] K. Dressler, Can. J. Phys. **47**, 547 (1969).
[4] P. K. Carroll and C. P. Collins, Can. J. Phys. **47**, 563 (1969).
[5] G. M. Lawrence, D. L. Mickey, and K. Dressler, J. Chem. Phys. **48**, 1989 (1968).
[6] D. Stahel, M. Leoni, and K. Dressler, J. Chem. Phys. **79**, 2541 (1983).
[7] D. Spelsberg and W. Meyer, J. Chem. Phys. **115**, 6438 (2001).
[8] J. Oddershede, N. E. Grüner, and G. H. F. Diercksen, Chem. Phys. **97**, 303 (1985).
[9] S. B. Ben-Shlomo, and U. Kaldor, J. Chem. Phys. **92**, 3680 (1990).
[10] D. C. Comeau and R. J. Bartlett, Chem. Phys. Lett. **207**, 414 (1993).
[11] S. J. A. van Gisbergen, F. Kootstra, P. R. T. Schipper, O. V. Gritsenko, J. G. Snijders, and E. J. Baerends, Phys. Rev. A **57**, 2556 (1998).
[12] D. J. Tozer and N. C. Handy, J. Chem. Phys. **109**, 10180 (1998).
[13] M. Grüning, O. V. Gritsenko, S. J. A. van Gisbergen, and E. J. Baerends, J. Chem. Phys. **116**, 9591 (2002).
[14] J. Pitarch-Ruiz, J. Sánchez-Marín, I. Nebot-Gil, and N. B. Amor, Chem. Phys. Lett. **291**, 407 (1998).
[15] P. R. T. Schipper, O. V. Gritsenko, S. J. A. van Gisbergen, and E. J. Baerends, J. Chem. Phys. **112**, 1344 (2000).
[16] O. V. Gritsenko, P. R. T. Schipper, and E. J. Baerends, Chem. Phys. Lett. **302**, 199 (1999).
[17] O. V. Gritsenko, P. R. T. Schipper, and E. J. Baerends, Int. J. Quantum Chem. **76**, 407 (2000).
[18] M. Nooijen, Int. J. Quantum Chem. **95**, 768 (2003).
[19] M. Nooijen, J. Chem. Phys. **104**, 2638 (1996).
[20] M. Nooijen and R. J. Bartlett, J. Chem. Phys. **106**, 6441 (1997).
[21] M. Nooijen and R. J. Bartlett, J. Chem. Phys. **106**, 6449 (1997).
[22] M. Nooijen and R. J. Bartlett, J. Chem. Phys. **107**, 6812 (1997).
[23] S. R. Gwaltney and R. J. Bartlett, J. Chem. Phys. **108**, 6790 (1998).
[24] M. Nooijen, Spectrochim. Acta, Part A **55**, 539 (1999).
[25] A. B. Parusel, G. Kohler, and M. Nooijen, J. Phys. Chem. A **103**, 4056 (1999).
[26] M. Nooijen and V. Lotrich, J. Chem. Phys. **113**, 494 (2000).
[27] Amsterdam density functional program, Theoretical Chemistry, Vrije Universiteit, Amsterdam, URL: http://www.scm.com
[28] G. te Velde, F. M. Bickelhaupt, E. J. Baerends, C. Fonseca Guerra, S. J. A. van Gisbergen, J. G. Snijders, and T. Ziegler, J. Comput. Chem. **22**, 931 (2001).
[29] A. D. Becke, Phys. Rev. A **38**, 3098 (1988).
[30] J. P. Perdew, J. A. Chevary, S. H. Vosko, K. A. Jackson, M. R. Pederson, D. J. Singh, and C. Fiolhais, Phys. Rev. B **46**, 6671 (1992).
[31] H. Köppel, W. Domcke, and L. S. Cederbaum, Adv. Chem. Phys. **57**, 59 (1984).
[32] L. S. Cederbaum, J. Chem. Phys. **78**, 5714 (1983).
[33] I. Özkan and L. Goodman, Chem. Rev. (Washington, D.C.) **79**, 275 (1979).
[34] E. J. Heller, Acc. Chem. Res. **14**, 368 (1981).
[35] E. J. Heller, R. L. Sundberg, and D. Tannor, J. Phys. Chem. **86**, 1822 (1982).
[36] A. B. Myers, Chem. Rev. (Washington, D.C.) **96**, 911 (1996).
[37] A. B. Myers, Acc. Chem. Res. **30**, 519 (1997).
[38] K. Ruedenberg and G. J. Atchity, J. Chem. Phys. **99**, 3799 (1993).
[39] A. Troisi and G. Orlandi, J. Chem. Phys. **118**, 5356 (2003).
[40] E. S. Kryachko and D. R. Yarkony, Int. J. Quant. Chem. **76**, 235 (2000).
[41] M. E. Casida, in *Recent Advances in Density Functional Methods Part I*, Time-Dependent Density Functional Response Theory for Molecules, edited by D. P. Chong (World Scientific, Singapore, 1995), pp. 155–192.
[42] S. J. A. van Gisbergen, J. G. Snijders, and E. J. Baerends, Comput. Phys. Commun. **118**, 119 (1999).
[43] M. Nooijen and A. Hazra, VIBRON–A program for Vibronic Coupling and

Franck–Condon calculations. With contributions from John Stanton and Kurt Sattelmeyer, University of Waterloo, 2003.
[44] A. J. Sadlej, Theor. Chim. Acta **79**, 123 (1991).
[45] A. J. Sadlej, Collect. Czech. Chem. Commun. **53**, 1995 (1988).
[46] T. H. Dunning, Jr., J. Chem. Phys. **90**, 1007 (1989).
[47] R. A. Kendall, T. H. Dunning, Jr., and R. J. Harrison, J. Chem. Phys. **96**, 6796 (1992).
[48] R. van Leeuwen and E. J. Baerends, Phys. Rev. A **49**, 2421 (1994).
[49] D. P. Chong, O. V. Gritsenko, and E. J. Baerends, J. Chem. Phys. **116**, 1760 (2002).
[50] S. Hirata and M. Head-Gordon, Chem. Phys. Lett. **314**, 291 (1999).
[51] C.-P. Hsu, S. Hirata, and M. Head-Gordon, J. Phys. Chem. A **105**, 451 (2001).
[52] D. J. Tozer, R. D. Amos, N. C. Handy, B. O. Roos, and L. Serrano-Andrés, Mol. Phys. **97**, 859 (1999).
[53] N. T. Maitra, F. Zhang, R. J. Cave, and K. Burke, J. Chem. Phys. **120**, 5932 (2004).